Plasma assisted deposition of single and multistacked TiO_2 hierarchical nanotubes photoanodes

A. Nicolas Filippin,[a]* Juan R. Sanchez-Valencia,[a] Jesús Idígoras,[b] T. Cristina Rojas,[c] Angel Barranco,[a] Juan A. Anta[b] and Ana Borras[a]*

We present herein an evolved methodology for the growth of nanocrystalline hierarchical nanotubes combining physical vapor deposition of organic nanowires (ONWs) and plasma enhanced chemical vacuum deposition of anatase TiO_2 layers. The ONWs act as vacuum removable 1D and 3D templates, occurring the whole process at temperatures ranging from RT to 250 ºC. As result, a high density of hierarchical nanotubes with tunable diameter, length and tailored walls microstructures are formed on a variety of processable substrates as metal and metal oxides films or nanoparticles including transparent conductive oxides. The reiteration of the process leads to the development of an unprecedented 3D nanoarchitecture formed by stacking layers of hierarchical TiO_2 nanotubes. As a proof of concept, we present the superior performance of the 3D nanoarchitecture as photoanode within an excitonic solar cell with efficiencies as high as 4.69% for nominal thickness of the anatase layer below 2.75 um. Mechanical stability and straightforward implementation in devices are at the same time demonstrated. The process is extendable to other functional oxides fabricated by plasma-assisted methods with readily applications in energy harvesting and storage, catalysis and nanosensing.

Introduction

One-dimensional (1D) nanomaterials like nanowires (NWs), nanotubes (NTs), nanorods (NRs) and nanofibers (NFs) are ubiquitous elements for the exploitation of fundamental nanotechnology applications. Their fabrication is crucial in aspects such as development of model systems for shape-dependent relationships and properties, miniaturization of components and tailored structure-enhanced performance.[1] Key advantage of the use of 1D materials is the ample variety in the modulation of their composition, shape and morphology to form complex nanoscale objects able to exhibit multiple functionalities.[1] Recent examples of heterostructured 1D nanomaterials comprise axial junctions,[1] radial junctions and core/shell nanostructures,[2-4] and multibranched and hierarchical nanowires (nanotrees) or networks.[5] In the latter cases, 1D nanostructures are assembled as three-dimensional (3D) architectures

showing even higher versatility in the composition modulation and a remarkable surface area. In a simplified way, the growth processes for the formation of 3D nanoarchitectures can be split in two main groups: i) multi-step sequential procedures usually including vapour-liquid-solid (VLS) or similar growth mechanisms and ii) the use of three dimensional templates.[5] General examples in the literature of 3D nanoarchitectures refer to the formation of inorganic crystalline nanowires[5-6] and networks formed by carbon nanofibers and nanotubes[7] with a relatively lower attention to the development of organic 3D scalfolds.8 In a further step, 3D nanostructures can be decorated with 0D materials (i.e. nanoparticles or quantum dots) to increase their functionality.[8b,e),9] This new generation of nanomaterials presents appealing properties in applications including catalysis, chemical and biochemical sensing, energy harvesting and storage, photonics and microelectronics.[5-9] In this context, we show herein an original template methodology that provides a reliable and simple way for the fabrication of 3D nanostructures with different levels of complexity, from hierarchical nanotubes (HNTs) with controlled wall microstructure, NTs forming nanotrees (NTrees) to finally, a multistack of nanotrees layers (NTrees-multistack). As a fundamental example of the possible applications of the 3D nanoarchitectures presented, here we show the formation of anatase TiO_2 nanomaterials with an enhanced performance as photoanode in dye-sensitized solar cells (DSCs). It is worth to stress herein that this protocol is straightforwardly extendable to the ample variety of materials composition and structures available by plasma assisted vacuum deposition technologies.[10]

Amorphous and anatase TiO_2 have been successfully employed in DSCs in the form of nanoparticles, nanosheets, nanotubes and nanowires achieving remarkable efficiencies by implementing optimized dyes and electrolytes.[11] Over the last few years, it has been demonstrated that TiO_2 nanoparticles suffer from relatively short electron diffusion lengths than 1D nanostructures due to the huge number of grain boundaries.[12] However, 1D nanostructures such as nanorods or nanowires offer much lower surface area compared to nanoparticles, hence dye concentration, and thereby photocurrent, are significantly lower in the latter case.[13] In order to achieve even higher efficiencies with TiO_2 systems, it is therefore required the development of structures with long diffusion lengths and high surface area. State of the art DSCs comprising 1D anatase nanostructures have achieved remarkable efficiencies of about 10% by implementing hierarchical anatase NWs.[11d] In other recent works, efficiencies between 4%-8% have been attained, always exploiting relatively thick hierarchical 1D nanostructures.[11c,13a,14] However, not less than 14 um or even 47 um of film thickness were needed for such high efficiencies. In this

article we will demonstrate an enhanced performance of the 3D photoanodes over their thin film and 1D counterparts achieving circa of 4.7% in efficiency for an equivalent thickness of the photoanode below 2.75 um. With such aim, the article is structured as follows. First, we present the fundamentals of a plasma/vacuum protocol for the fabrication of hierarchical anatase TiO_2 using organic nanowires as 1D/3D template and further development of unprecedented nanotrees-multistack nanoarchitectures. Secondly, we report on the fabrication and characterization of dye sensitized solar cells based on these novel materials.

Results and discussion

Fabrication of anatase hierarchical nanotubes

Scheme 1 and Figure 1 gather the different vacuum and plasma deposition and processing steps involved in the formation of anatase hierarchical nanotubes (HNTs). The most important and original characteristic of this method is the use of single crystalline organic nanowires (ONWs) as vacuum processable 1D templates for the formation of hybrid nanowires or metal oxide nanotubes with tailored microstructured walls. The ONWs are formed by small molecules (porphyrins and phthalocyanines) that are relatively low cost precursors.[15] The removal of the template is carried out under mild solventless conditions.[16] Thus, the first two steps (0 and i) are related to the formation of the ONWs on processable substrates. Step 0) is the fabrication of a seed layer, required for highly dense and homogeneous ONWs growth.[17] As published elsewhere,[17a-c)] the seed layer roughness instead of its chemical composition is the critical parameter to prompt the formation of ONWs. Such surface roughness or grains dispersion acts as nucleation centres for the single-crystal formation under supersaturation conditions, driven by the strongly directional π-stacking self-assembly.[17d,18] Herein, looking to the final application of the HNTs as photoanode in dye solar cells (where a blocking layer between FTO and electrolyte is desirable), we have selected as seed layer a polycrystalline anatase film (ca. 200 nm) grown by plasma enhanced chemical deposition (PECVD).[19] Step i) represents the physical vacuum deposition (PVD) process that provides the growth of squared ONWs and nanobelts. Growth conditions such as substrate temperature and growth rate depends on the chemical structure of the small-molecule forming the ONWs.[17] In this work, we have utilized phthalocyanine molecules (H_2Pc) with a relative high sublimation temperature (above 250 ºC) under the our settled vacuum conditions (see Experimental and Electronic Supplementary Information (ESI) Sections). As result, ONWs in a density about 10 NW x um^{-2} with tuneable

lengths in the range between 1 and 30 um and diameters between 50 and 120 nm are formed (see Figure 1 a). Density, length and diameter of the ONWs strongly depend on the growth time.[17] The third step (Step ii) represents the conformal deposition by PECVD of the titanium dioxide shell on the as-grown ONWs (Scheme 1 and Figure 1 b) in order to form hybrid ONW@TiO_2 1D nanostructures. In recent articles, we have proved this procedure for the formation of nanoporous TiO_2 and SiO_2 and polycrystalline ZnO shells at room temperature.[16,20] In order to provide the formation of crystalline TiO_2 we have applied the conditions reported for the formation of anatase thin films by PECVD.[19] It is important to address that the temperature required for the formation of the anatase layer (250 ºC) is close to the sublimation temperature of the H_2PC small-molecule. Therefore, the direct deposition of the TiO_2 at 250 ºC on the ONWs used as 1D scaffolds would eventually lead to their sublimation and evacuation. In order to overcome this handicap, we firstly produce a thin TiO_2 shell (below 50 nm) at 150 ºC as interlayer to preserve the 1D scaffold and then

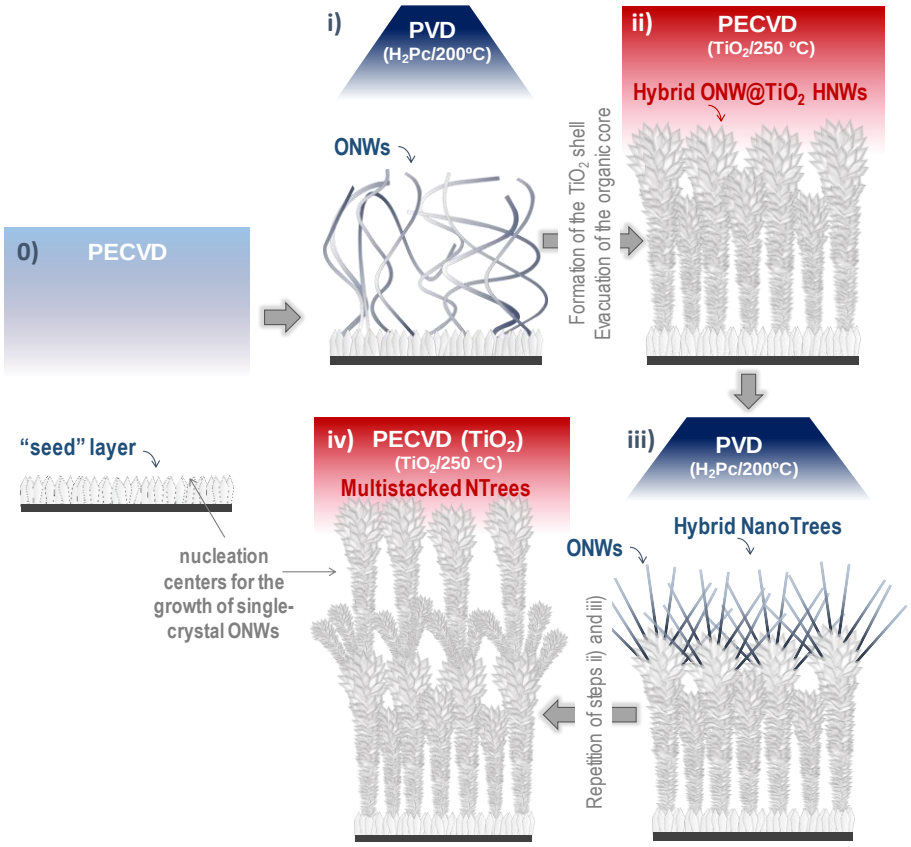

Scheme 1. Schematic representation of the different steps in the multistacked nanotrees fabrication, namely, i) PVD of pi-conjugated molecules to form ONWs; ii) conformal growth of anatase shell at 250 ºC and consequent formation of hierarchical TiO2 nanotubes (HNTs); iii) secondary growth of ONWs on the HNTs; iv) reiterative reproduction of steps ii) and iii) to form a multistack.

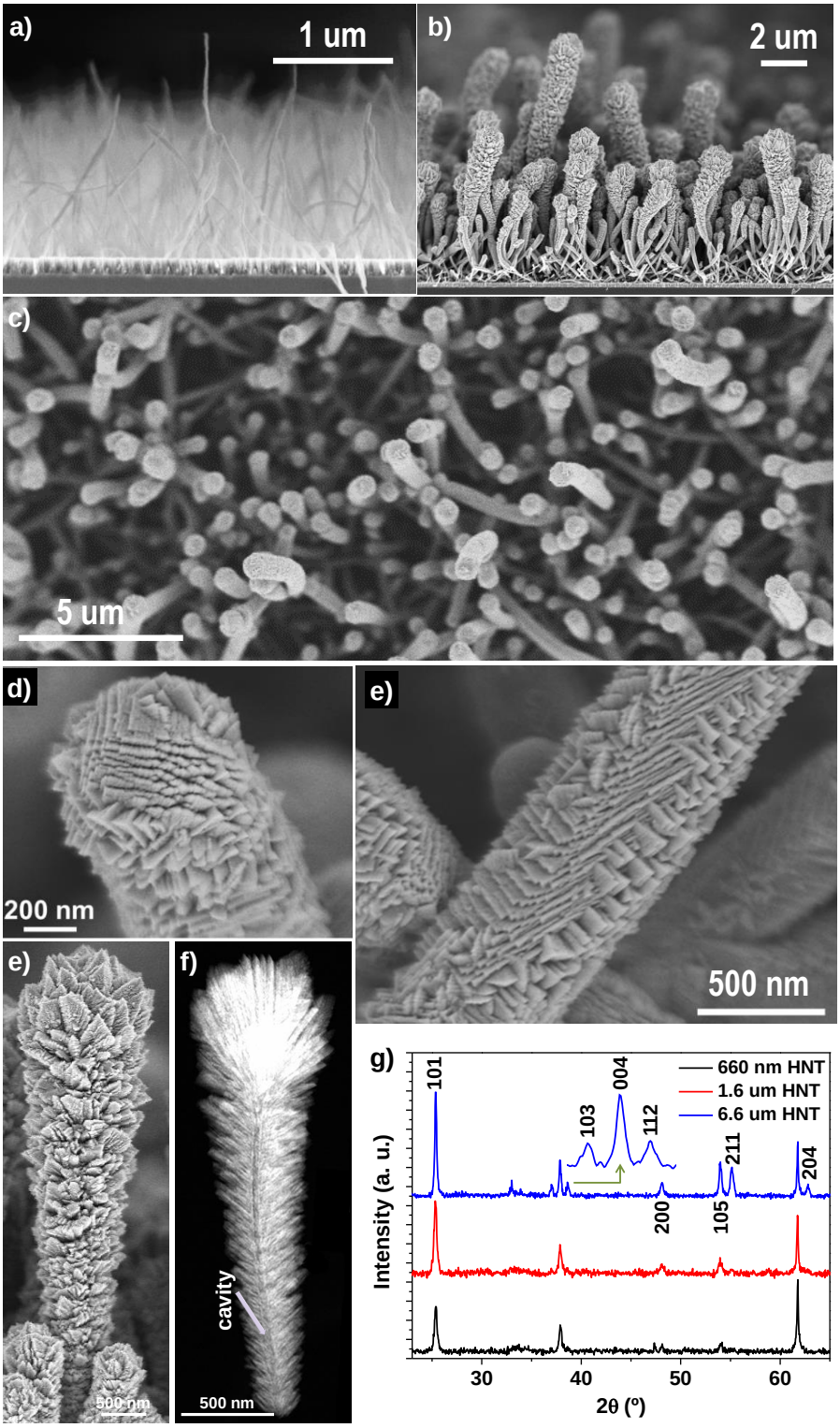

Figure 1. a) Characteristic cross-section SEM image showing the formation of H_2Pc single crystal organic nanowires using an anatase film as seed layer. (b-c) Cross-section and normal view SEM micrographs of a 1.6 and 660 nm anatase HNT-films correspondently. Details of a 660 nm -HNT tip and lateral appear in d-e); (e-f) SEM and HAADF-STEM images of a 1.6 um HNT; g) XRD diagrams of HNTs with different thicknesses.

increase the substrate temperature until 250ºC. In this way, the final deposition of the anatase shell occurs at the same time that the organic core sublimation and evacuation. In this way, the final 1D nanostructures depict the form of domed-nanotubes (Figure 1 b-f) with a sharp and flat inner interface with the emptied core. It is important to stress that the deposition of the inorganic shell by PECVD leads to the vertical alignment of the nanowires (Figure 1 b-c) otherwise randomly oriented (Figure 1 a). Such alignment responds to a combination of the electrostatic repulsion between the ONWs under effect of the electric field in the plasma sheath and to the increment of the rigidity of the nanowires because of the metal oxide shell formation.[20] Final diameter of the HNTs is controllable through the growth rate and deposition time of the anatase shell. In order to facilitate the comparison between samples, we denote them after their nominal thickness, i.e. the actual thickness of the thin film grown under identical conditions on flat reference samples (Si(100), fused silica slides and FTO, see Figure S1 in the Electronic Supplementary Information). Keeping in mind the final application of the anatase nanotubes

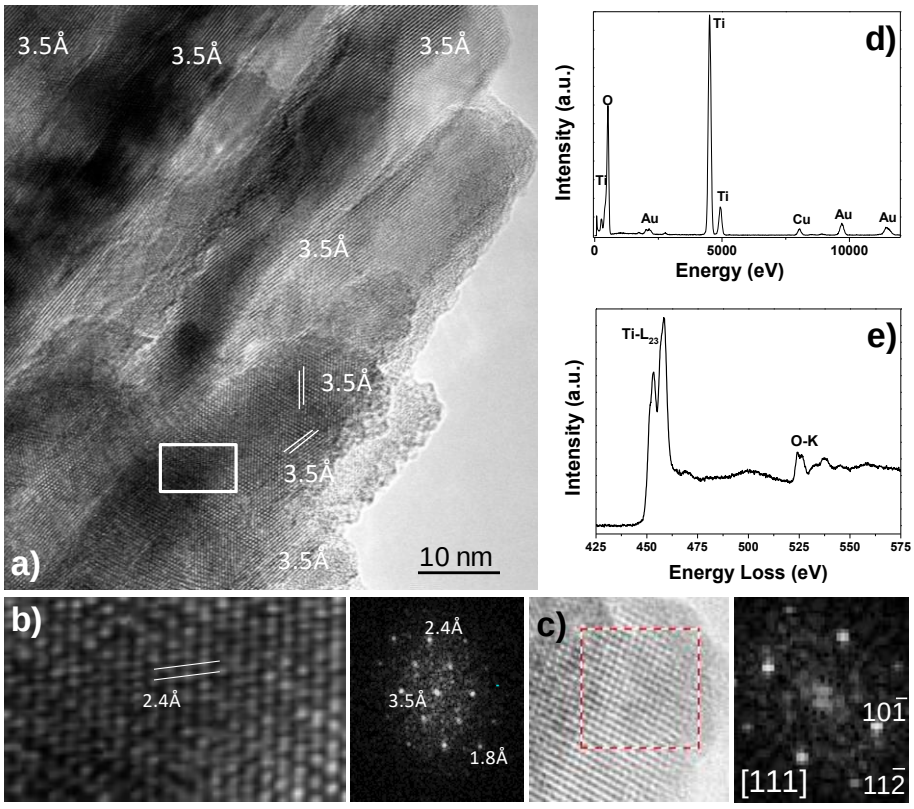

Figure 2. a) HREM images of a 660 nm HNT, labels address the 3.5Å interplanar spacing assigned to (101) planes; b) focus-in image of the selected area in a) and corresponding DDP revealing interplanar distances compatibles with (004) planes; c) HREM and DDP of a grain showing (101) and (112) planes for the selected region in the insets. (d-e) EDX and EELS spectra revealing the composition of the nanotubes (see also XPS results in ESI section).

as photoanode in excitonic solar cells, we have selected three different nominal thicknesses: 660 nm, 1.6 um and 6.6 um. Figure 1 d-f) presents SEM and HAADF-STEM images of the 660 nm- (a-e) and 1.6 um- (e-f) anatase nanotubes showing for both nominal shell thicknesses a marked crystalline nanostructure with features growing radially and axially from the NT core. The microstructure of the shell is similar to that of anatase thin films grown directly on Si substrates[19] (Figure S1). In fact, by a close inspection to Fig. 1 d-f), it may be noted that each crystal emerging from the NT is decorated with numerous sub-crystals, resembling a feather, thus giving rise to a hierarchical nanotube (HNT). The anatase feathers growing radially from the axis of the HNTs retained some degree of individuality with some empty space between them as evidenced by HAADF-STEM in Figure 1 f). However, they grow connected at the bottom forming the cavity walls, providing the structural integrity needed after the sublimation of the organic core. On the other hand, the diameter of the HNTs was not uniform along the whole structure appearing thicker at the top and gradually thinner towards the base (Fig. 1 e-f). Such characteristic responds to the shadowing effect of the nanowires tip during the growth of the inorganic shell and it is therefore more pronounced for NTs with bigger diameters.[21] For the highest diameter of the anatase shell (6.6 µm equivalent thickness), the HNTs heads collapse (see Figure S2). Thus, the gaps between adjacent structures are reduced dramatically to the extent of a noticeable percolation at the top. Moreover, it is worth mentioning that these structures presented a high degree of interconnection at the interface with the substrate (Figure S2). Table S1 gathers the mean HNTs lengths showing that even for the highest nominal thickness of the anatase shell, the average HNT length stays below 10 µm. Figure 1 g) and Figure S3 summarize XRD diagrams for HNTs layers and thin films correspondently clearly evidencing the crystalline anatase phase. Texturization of the thin films along the planes (112) and (211) is deduced from the relative peak intensities in the diffractograms (see also reference 19). The crystallite size, calculated by the Scherrer method (Table S2), remains below 100 nm for all the samples under study. These results are in good agreement with the High Resolution Electron Microscopy (HREM) characterization gathered in Figure 2. The image in panel a) shows the tips of the feathers forming the columnar shell of a 660 nm – HNT. Most of the grains in this image present an interplane spacing of 3.5 Å compatible with planes (101).[22] The spatial resolution of our set-up (2.5 Å) hampers a clear determination or smaller interplanar spacing. However, in the focus-in image in b) and the Digital Difractogram Pattern (DDP) on the left reveal distances ca. 2.4 Å compatible with the presence of (004).[22] HREM in the tip of a feather-like column gathered in panel c) and the corresponding DDP are

compatible with two family of planes (101) and (112).[22] On the other hand, EDX and EELS spectra in Figure 2 d-e) along to the XPS characterization in Figure S4 further support the formation of TiO_2 and complete evacuation and removal of the organic molecules forming the ONW from the HNTs surface. XPS survey spectrum in Figure S4 presents peaks corresponding to Si (from the silicon wafer used as substrate), C, Ti and O. We found no trace of nitrogen associated to the H_2Pc detection. The estimated atomic percentages (65 % for oxygen, 22% for Ti and 13% for C) and the low content in C in EDX spectra indicate the complete oxidation of the organometallic TTIP precursor during the PECVD process (see experimental). Additional presence of carbonaceous species likely corresponds to spurious carbon contamination after handling the samples in air.

Fabrication of anatase Nanotrees-multistack

As mentioned above, formation of 3D architectures as networks or nanotrees represent a significant advance in the development of multifunctional nanomaterials for energy harvesting.[1-6] Thus, one of the most interesting characteristics of these 3D nanomaterials is that the branches and stems act as direct pathway for charge and light and enormously enhance the surface area respect to the 1D counterpart.[5] Furthermore, the lateral connectivity can be also greatly improved which is very profitable from the point of view of the implementation of these nanomaterials within electronic and optoelectronic devices. Within such appealing framework, we propose herein a new type of 3D architecture (Figure 3) consisting in the stack of anatase HNTs layers. The underlying idea behind this approach consists in the use of the nanoscale features at the as-grown HNTs surface as nucleation centres for the formation of secondary organic nanowires (see Scheme1, Step iii). Due to geometrical constraints, the secondary ONWs growth is preferential at the tips of the HNTs (see Fig. 3 a-b) although for the longer nanotubes the ONWs decoration can be also visible covering their overhanging section (Figure 3c). Secondary ONWs grow axially distributed from the as-grown HNTs forming hybrid nanotrees. Step iv) consists in the repetition of Step ii) to form an anatase layer to cover the new organic nanowires. The deposition of the TiO_2 shell takes place conformal to the tallest ONWs with little increment in the diameter of the previously formed HNTs because of shadowing effects. In addition, secondary ONWs not covered by TiO_2 sublimate at the given 250 ºC. Such experimental methodology contributes to the homogeneity and reproducibility in length, thickness and density distributions between consecutive HNTs layers. The protocol is then repeated adding layers to develop the multistacked nanotrees architecture. Figure 3 e) shows the result of a three-layers multistack with a total equivalent thickness ca. 2.75 um (850 nm for the first two layers and 1 um for the third one, see equivalent thin film in Figure S5).

HNTs and NTrees-multistack solar cells

In this section, we evaluate the application of HNTs and NTrees-multistack as photoanodes in dye-sensitized solar cells. Firstly, we need to reproduce such nanoarchitectures and probe their mechanical stability on transparent conducting oxides (TCOs) supports such as FTO. Thus, the fabrication and assembly of the solar cell follows the steps shown in Scheme 1 where a 200 nm anatase layer deposited in Step 0) plays a double role, such as seed layer for the formation of ONWs and as a blocking layer between the liquid electrolyte and the TCO. Figure 4 a) shows the different stages in the cell preparation and assembly. First, we follow to summarize the optical properties of the HNTs and NTrees samples in comparison to the thin films deposited as reference. Figure S6 presents the UV-Vis-NIR transmission spectra of a 3 um thick anatase thin film and the corresponding HNTs sample. The latter strongly scatter the light in the visible and NIR range, whereas the thin film presents a significant higher transparency. This is the general trend for all the cases, with thin film samples showing a high transparency meanwhile, HNTs exhibit always a whitish appearance (see step 4 in Figure 4 a) due to noticeable light scattering effects. This property is highly desirable for the DSC performance optimization since it increases the photon absorption and, therefore, light harvesting.[11d,23] Figure S7 shows the comparison between HNT and thin film samples after step 5) in order to illustrate the effect of the HNT formation on the dye loading capability. As expected, these results indicate that the thicker the nominal thickness of the anatase shell the greater the amount of dye adsorbed with HNT samples. Thus, HNTs exhibited always a more intense pigmentation than their equivalent thin film in good agreement with the surface area enhancement for the 1D configuration.

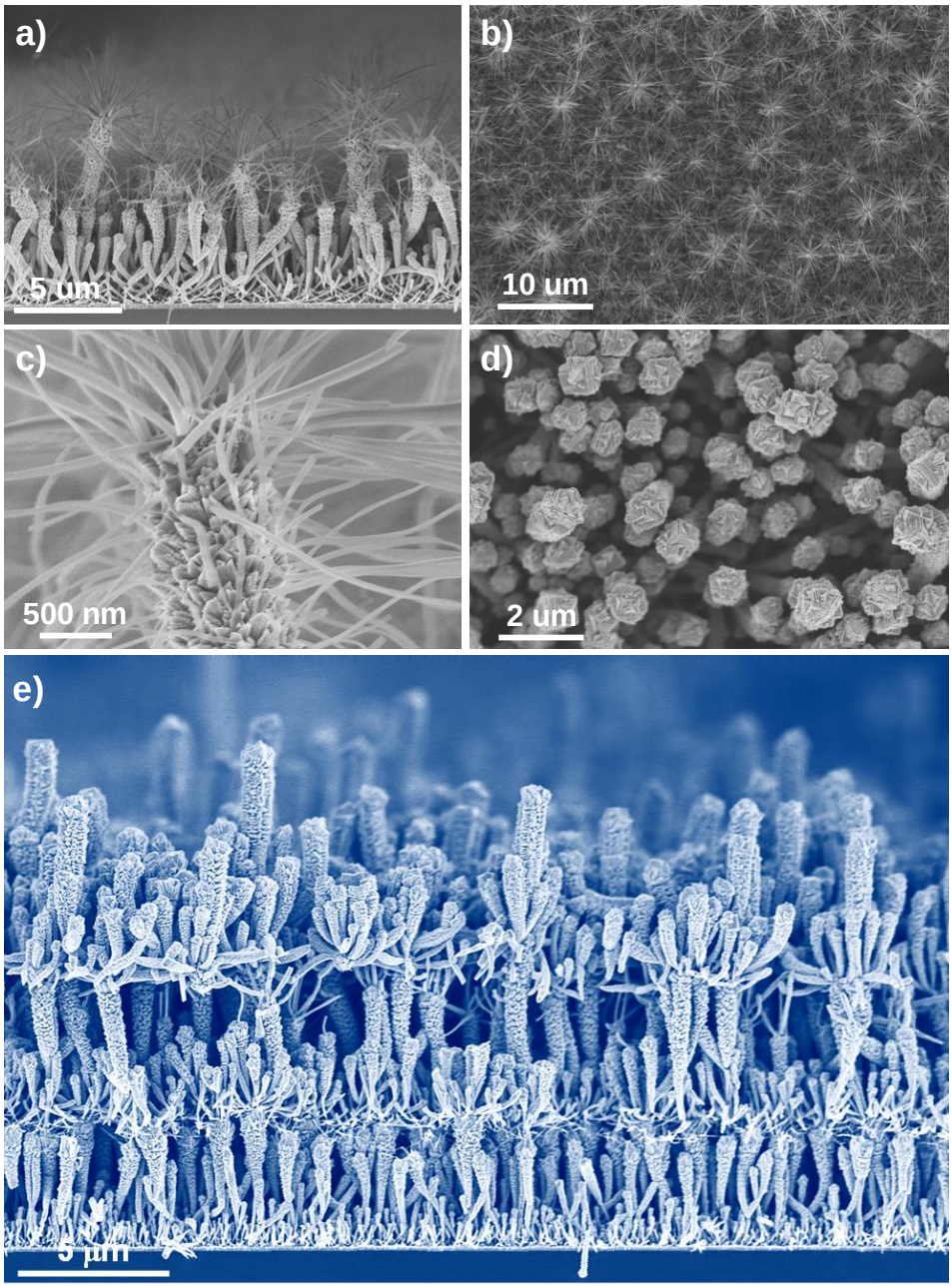

Figure 3. Characteristic SEM images of the different steps in the multistacked nanotrees formation.

The increment in dye loading for HNTs devices translates into higher photocurrents (JSC) in comparison with thin films and raising with the HNTs equivalent thickness (see Figure 4b) and Table 1). The pronounced light dispersion in HNTs layers is likely contributing as well to the high photocurrent values. On the other hand, the photovoltage (VOC) also increases with the thin film thickness reaching a maximum of 831±1 mV for the 6.6 um sample. This same behaviour was previously reported for ZnO thin films grown by PECVD.[24] V_{OC} values for HNTs cells are slightly dependent on the shell nominal thickness, but are much larger than those of equivalent thin film cells for low thicknesses.

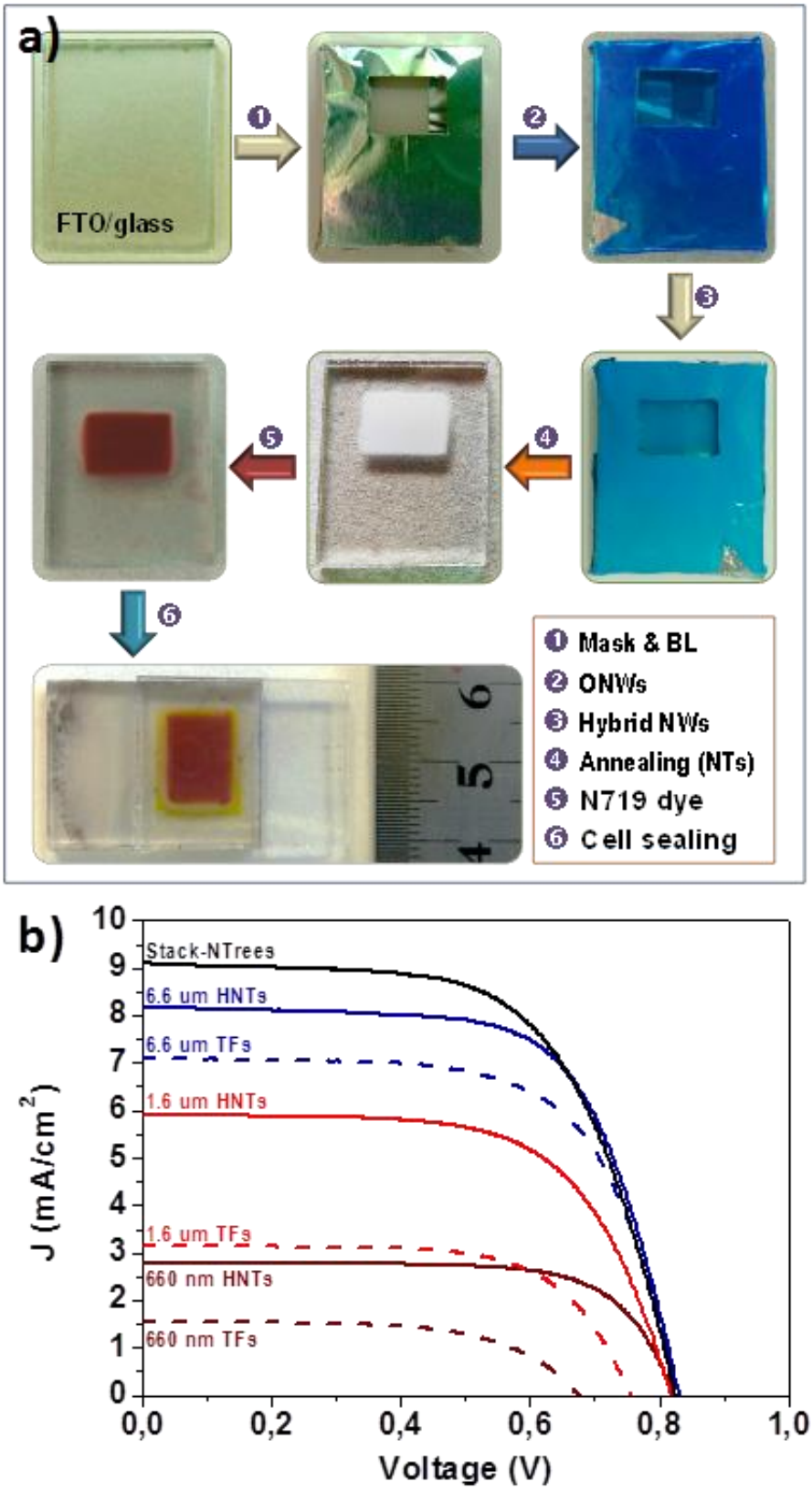

Figure 4. a) Photographs showing the different steps of the DSC fabrication; b) I-V curves for the DSCs assembled with HNTs and TFs of three wall thicknesses, and the multistacked nanotrees (best cells shown).

This trendy indicates a substantially low recombination rate for HNTs photoanodes. In addition, the fill factor (FF) does not change significantly with the thickness in the thin film cells, while for HNTs it decreases as the thickness increases. This latter aspect correlates with the higher photocurrents and associated series resistance voltage drops. Interestingly, HNTs exhibited a higher fill factor than thin films.

For the highest thickness, 6.6 um, the efficiency of the thin film cell nearly triplicates, whereas for HNTs it augmented by a factor of 1.5. It is important to address herein that the increment of the HNTs diameters is strongly affected by self-shadowing effects as addressed above. Correspondently, the percolation level between the tips of the nanotubes also increases (Figure S2). The next step is, therefore, to apply the 3D approach based on the NTrees-multistack in Figure 3 to overcome this issue. In this way, we take advantage of the enhancement in surface area with no detriment in the effective charge transport. Accordingly, the NTrees-multistack samples show an exceptional photovoltaic performance, achieving an average value of efficiency of 4.69%. In spite of the fact that the total length of the stack was around 14 um,

Table 1. Photovoltaic parameters for TiO_2 (anatase)-based DSCs as a function of the equivalent thickness - Mean photovoltaic parameters values and estimated errors have been obtained from data of three devices with the same configuration. Thin film thickness corresponds to the nominal thickness of the HNTs, i.e. fabricated under the same experimental conditions on a flat substrate.

Cell	J_{sc} (mA/cm^2)	V_{oc} (mV)	*FF* (%)	η (%)
660 nm TF	1.52±0.05	670±7	62.7±1.9	0.64±0.05
1.6 um TF	2.86±0.30	698±58	64.9±1.4	1.31±0.27
6.6 um TF	7.12±0.15	831±1	63.6±1.6	3.76±0.17
660 nm HNTs	2.48±0.30	833±9	71.4±0.8	1.47±0.10
1.6 um HNTs	5.39±0.53	819±2	66.6±2.4	2.93±0.18
6.6 µm HNTs	7.87±0.58	835±6	65.7±0.2	4.32±0.30
Multistack (2.75 um)	9.19±0.17	824±5	61.9±1.0	4.69±0.10

the thickness of the equivalent anatase thin film was only 2.75 um. In addition, the photocurrent is remarkably high, likely result of a successful combination of high surface area, scattering and light trapping effects. We have analysed the different transport process parameters by means of Electrochemical Impedance Spectroscopy (EIS) and modelling. Figure S8 includes the results comparing[25] the cells with highest efficient, i.e. 6.6 um TF, 6.6. um HNT and NTrees-multistack. The exponential behaviour evidences that a chemical capacitance is controlling accumulation in the TiO_2[26] being larger for the stack, as expected for higher surface areas. It is also noticeable that the largest recombination resistance (R_{res}) corresponds also to the NTrees-multistack. The electron lifetime (τ_n) trends agree with the obtained potentials in the I-V curves: the longer the electron lifetime the higher the V_{OC} and vice versa. Diffusion coefficients (D_n) were estimated by Intensity-Modulated Photovoltage Spectroscopy (IMPS) (Figure S9). This parameter is slightly higher for the stack and lower for the thicker HNTs (6.6 um). Attending to the curves shape

(straight lines) we assume a multiple trapping transport mechanism.[27] By combining the electron lifetime obtained from EIS data and the diffusion coefficient from IMPS, the electron diffusion length for each cell might be estimated through equation $L_n=\sqrt{(D_n \times \tau_n)}$ (Figure S9). For all the cases, the diffusion length is at least 10 times greater than the photoanode thickness indicating a collection efficiency of a 100%. This confirms that the main advantage of the hierarchical nanostructures is to increase the surface area for dye adsorption without affecting significantly the good transport properties of the anatase hierarchical shells.

Experimental Section

ONWs by PVD. The organic precursor Phthalocyanine (H_2Pc) was supplied from Aldrich and used as received without further purification. The PVD procedure for the formation of single crystal ONWs has been fully described in previous references.[17] It consists on the sublimation of the organic molecules from a Knudsen cell at 0.02 mbar of Ar using a growth rate about 0.3 Å/s and controlled substrate temperature (~200 ºC).

TiO_2 layers by PECVD. Anatase layers and shells were fabricated in a microwave (2.45 GHz) ECR reactor with a down-stream configuration using titanium tetraisopropoxide (TTIP) as precursor. Total pressure in the chamber was settled at 1.5 x 10^{-2} mbar and plasma power at 400 W keeping the subtrates at 250 ºC during the fabrication process. An intermediate layer was formed at 150 ºC to be used as 1D scaffold previous to the organic core sublimation during the anatase deposition.

Fabrication of the anatase multistack. The NTrees-multistack were produced by a consecutive deposition process. A first layer of NTs was produced growing 0.65 kÅ (measured in the quartz crystal monitor (QCM)) of H_2Pc using an anatase thin film (200 nm) as seeds for ONWs (it also acts as blocking layer for the DSC), followed by the deposition of 860 nm of anatase. This process was repeated two more times increasing the thickness of the deposited anatase in a total of 2.75 um.

Dye-Sensitized Solar cells fabrication procedure and characterization. Section S1 in the Electronic Supplementary Information section gathers the detailed process.

Characterization. SEM micrographs were acquired in a Hitachi S4800 working at 2 kV. The samples were dispersed onto Holey carbon films on Cu or Ni grids from Agar scientific for TEM characterization. The HREM images were obtained in an S/TEM FEG-TALOS FS 200S de FEI, working at 200KV with 2.5 nm point resolution. The HAADF-STEM image was obtained with a

FEG S/TEM Tecnai G2F30 from FEI, working at 300 kV, equipped with a high angle annular dark field (HAADF) detector from Fischione with a 0.16 nm point resolution. X-EDS spectra were recorded with an XEDS detector SSD (INCA X-Max 80), and Electron energy-loss spectroscopy (EELS) using a Gatan Imaging Filter (GIF) (QUAMTUM SE model). UV-VIS-NIR spectra were recorded in PerkinElmer Lambda 750 UV/Vis/NIR spectrophotometer. The crystal structure was analysed by XRD in a Panalytical X'PERT PRO spectrometer operated in the θ - 2 θ configuration and using the Cu Kα (1.5418 Å) radiation as an excitation source. The crystallite size was determined with PANalytical X'Pert HighScore Plus software, which employs the Scherrer equation for the calculations.

Conclusions

We have demonstrated a reliable full vacuum/plasma methodology based on the use of supported ONWs as 1D and 3D template for the fabrication of hierarchical anatase nanotubes and multistacked nanotrees layers. This template method provides different advantages for the straightforward implementation of these 1D and 3D nanoarchitectures in electronic and optoelectronic devices: compatibility in an ample variety of materials, including TCOs; mild and solventless conditions for template removal on the substrate and fine control on the shell microstructure and composition (see also reference 16). To the best of our knowledge, this is the first time that a nanoarchitecture such as the NTrees-multistack developed by a full dry approach at temperatures below 250 ºC is reported. In order to probe the enhancement in surface area, improvement of the electrical connectivity and direct charge transport for this evolved approach we have successfully built HNTs and NTrees-multistack solar cell-photoanodes. These 1D and 3D cells outperformance the thin films counterparts showing as well a proper mechanical stability. It is also interest to stress that an active area as big as 0.7 cm^2 was achieved with an appreciable homogeneity (see Figure 4). Moreover, the 3D nanoarchitectures reached an efficiency of 4.69% with a relatively low TiO_2 thickness (2.75 um). Such a promising value responds to the combination of high light scattering, enhanced dye loading and conservation of the electron transport properties of the anatase shells. It is interesting to address that the multistacked nanotrees can easily progress to contain different shells nanostructures selecting the deposition conditions during the shell growth. It is also possible to extend the formation to multishell-nanotubes[16] as well as combining layers of NTs with different composition. These successful results and the straightforward extension of this template

method to the growth of plasma assisted deposited functional shells (including metal and metal oxide materials)[10] with tailored nanostructures and properties will certainly lead the path to the development of a new generation of 3D nanoarchitectures with appealing applications in energy harvesting, conversion and storage, nanosensing and catalysis.

Acknowledgements

We thank the Junta de Andalucia (FQM 1851 and FQM-2310) and the Spanish Ministry of Economy and Competitiveness and Agencia Estatal de Investigación (MAT2016-79866-R, MAT2013-40852-R, MAT2013-42900-P, MAT2013-47192-C3-3-R, MINECO-CSIC 201560E055 and Red de Excelencia "Emerging photovoltaic Technologies") and the EU through cohesion fund and FEDER programs for financial support. We also thank the Laboratory for Nanoscopies and Spectroscopies (LANE) at the ICMS and the General Services for Research and CITIUS from the University of Seville for the Advanced TEM characterization. JRS-V and AngelB acknowledge funding from EU project *PlasmaPerovSol*. This project has received funding from the European Union's Horizon 2020 research and innovation programme under the Marie Skłodowska-Curie grant agreement No 661480.

Notes and references

1 a) P. Yang, R. Yan and M. Fardy *Nano Lett.,* 2010, **10**, 1529; b) A. J. Mieszawska, R. Jalilian, G. U. Sumanasekera and F. P. Zamborini *Small,* 2007, **3**, 722; c) S. K. Kim, X. Zhang, D. J. Hill, K. D. Song, J. S. Park, H. G. Park and J. F. Cahoon *Nano Lett.,* 2015, **15**, 753; d) M. Yao, N. Huang, S. Cong, C. -Y. Chi, M. A. Seyedi, Y. –T. Lin, Y. Cao, M. L. Povinelli, P. D. Dapkus and C. Zhou *Nano Lett.*, 2014, **14**, 3293; e) N. P. Dasgupta, J. Sun, C. Liu, S. Brittman, S. C. Andrews, J. Lim, H. Gao, R. Yan and P. Yang *Adv. Mater.,* 2014, **26**, 2137; f) A. Zhang, C. M. Lieber *Chem. Rev.* 2016, *116*, 215; g) S. Mitragotri, D. G. Anderson, X. Chen, E. K. Chow, D. Ho, A. V. Kabanov, J. M. Karp, K. Kataoka, C. A. Mirkin, S. H. Petrosko, J. Shi, M. M. Stevens, S. Sun, S. Teoh, S. S. Venkatraman, Y. Xia, S. Wang, Z. Gu and C. Xu *ACS Nano,* 2015, **9**, 6644; j) C. M. Cobley, J. Chen, E. C. Cho, L. V. Wang and Y. Xia, *Chem. Soc. Rev.* 2011, **40**, 44; k) S. Hoang and P. X. Gao *Adv. Energy Mater.,* 2016, **6**, 1600683.

2 a) P. D. Cozzoli, T. Pellegrino and L. Manna *Chem. Soc. Rev.,* 2006, **35**, 1195; b) C. M. Lieber and Z. L Wang *MRS Bulletin,* 2007, **32**, 99; b) S. Misra, L. Yu, W. Chen, M. Foldyna and P. Pere Roca i Cabarrocas *J. Phys. D,* 2014, **47**, 393001.

3 a) L. Bao, J. Zang, X. Li *Nano Lett.* 2011, **11**, 1215; b) L. E. Greene, M. Law, B. D. Yuhas and P. Yang *J. Phys. Chem. Lett.,* 2007, **111**, 18451; c) O. Hayden, A. B. Greytak and D. C. Bell *Adv. Mater.,* 2005, **17**, 701; d) A. Walther, J. Yuan, V. Abetz and A. H. E. Müller *Nano Lett.,* 2009, **9**, 2026; e) A. Borras, A. Barranco and A. R. Gonzalez-Elipe *Langmuir,* 2008, **24**, 8021.

4 a) Y. C. Pu, G. Wang, K. D. Chang, Y. Ling, Y. K. Lin, B. C. Fitzmorris, C. M. Liu, X. Lu, Y. Tong, J. Z. Zhang, Y. J. Hsu and Y. Li *Nano Lett.,* 2013, **13**, 3817; b) S. Su, X. Wei, Y. Zhong, Y. Guo, Y. Su, Q. Huang, S. T. Lee, C. Fan and Y. He *ACS Nano,* 2012, **6**, 2582; c) Z. Zhang, A. Li, S.W. Cao, M. Bosman, S. Li and C. Xue *Nanoscale,* 2014, **6**, 5217; d) X. Zou, J. Wang, X. Liu, C. Wang, Y. Jiang, Y. Wang, X. Xiao, J. C. Ho, J. Li, C. Jiang, Y. Fang, W. Liu and L. Liao *Nano Lett.,* 2013, **13**, 3287-3292.

5 a) C. Cheng and H. J. Fan *Nano Today,* 2012, **7**, 327-343; b) E. Makarona, M.C. Skoulikidou, Th. Kyrasta, A. Smyrnakis, A. Zeniou, E. Gogolides and C. Tsamis *Mater. Lett.,* 2015, **142**, 211; c) K. Ravi and J. J. Schneider *Chem. Soc. Rev.,* 2012, **41**, 5285; d) Li Y. J., Yan Y., Zhang C., Zhao Y. S. and Yao, J. *Adv. Mater.* 2013, **25**, 2784; e) Y. Zhao, L. Fan, Y. Zhang, H. Zhao, X. Li, Y. Li, L. Wen, Z. Yan and Z. Huo *ACS Appl. Mater. Inter.,* 2015, **7**, 16802.

6 a) S. H. Bae, J. E. Kim, H. Randriamahazaka, S. Y. Moon, J. Y. Park and I. K. Oh *Adv. Energy Mater.,* 2017, **7**, 1601492; b) L. Q. Mai, F. Yang, Y. L. Zhao, X. Xu, L. Xu and Y. Z. Luo *Nature Comm.,* 2011*,* **2**, 381.

7 a) M. D. Volder, S. H. Tawfick, S. J. Park, D. Copic, Z. Zhao, W. Lu and A. J. Hart *Adv. Mater.* 2010, **22**, 4384; b) Y. Cheng, L. Huang, X. Xiao, B. Yao, L. Yuan, T. Li, Z. Hu, B. Wang, J. Wan and J. Zhou *Nano Energy* 2015, **15**, 66.

8 a) J. T. Korhonen, P. Hiekkataipale, J. Malm, M. Karppinen, O. Ikkala and R. H. A. Ras *ACS Nano,* 2011, **3**, 1967; b) N. G. Cho, H. S. Woo, J. H. Lee and I. D. Kim *Chem. Commun.,* 2011, **47**, 11300; c) I. J. Yuan, P. X. Zhu, N. Fukazawa and R. H. Jin *Adv. Funct. Mater.,* 2006, **16**, 2205; d) R. Garifullin, H. Eren, T. G. Ulusoy, A. K. Okyay, N. Biyikli and M. O. Guler *Phys. Status Solidi A,* 2016, **213**, 3238; e) M. A. Khalily, H. Eren, S. Akbayrak, H. H. Susapto, N. Biyikli, S. Ozkar and M. O. Guler *Angew. Chem. Int. Ed.,* 2016, **55**, 12257.

9 a) P. Sudhagar, T. Song, D. H. Lee, I. Mora-Sero, J. Bisquert, M. Laudenslager, W. M. Sigmund, W. I. Park, U. Paik and Y. S. Kang *J. Phys. Chem. Lett.,* 2011, **2**, 1984; b) M. C. Gutierrez, M. J. Hortiguela, J. M. Amarilla, R. Jimenez, M. L. Ferrer and F. Monte *J. Phys. Chem. C*, 2007, **111**, 5557.

10 a) K. Ostrikov, U. Cvelbar and A. B. Murphy *J. Phys. D: Appl. Phys.,* 2011, **44**, 174001; b) K. Ostrikov, E. C. Neyts and M. Meyyappan *Adv. Phys.,* 2013, **62**, 113; c) N. Donato and G. Neri

Nanosci. Nanotechnol. Lett., 2012, **4**, 211–227; d) A. Nasonova and K. S. Kim *RSC Adv.,* 2014, **4**, 29866; e) S. K. Sharma, S. Barthwal, V. Singh, A. Kumar, P. K. Dwivedi, B. Prasad and D. Kumar *Micron,* 2013, **44**, 339; f) F. J. Aparicio, M. Holgado, A. Borras, I. Blaszczyk-Lezak, A. Griol, C. A. Barrios, R. Casquel, F. J. Sanza, H. Sohlström, M. Antelius, A. R. Gonzalez-Elipe and A. Barranco *Adv. Mater.,* 2011, **23**, 761; g) A. Barranco, A. Borras, A. R. Gonzalez-Elipe and A. Palmero *Prog. Mater. Sci.,* 2016, **76**, 59; h) L. Martinu and D. Poitras *J. Vac. Sci. Technol. A,* 2000, **18**, 2619; i) E. Makarona, M. C. Skoulikidou, Th. Kyrasta, A. Smyrnakis, A. Zeniou, E. Gogolides and C. Tsamis *Materials Letters,* 2015, *142*, 211; j) U. Cvelbar *J. Phys. D.,* 2011, *44*, 17.

11 a) D. Chen, F. Huang, Y. B. Cheng and R. A. Caruso *Adv. Mater.,* 2009, **21**, 2206; b) J. Yu, J. Fan and K. Lv *Nanoscale,* 2010, **2**, 2144; c) J. Y. Liao, B. X. Lei, H. Y. Chen, D. B. Kuang and C. Y. Su *Ener. Environm. Sci.,* 2012, **5**, 5750; d) W. Q. Wu, Y. F. Xu, C. Y. Sua and D. B. Kuang *Ener. Environm. Sci.,* 2014, **7**, 644; e) A. Yella, H. W. Lee, H. N. Tsao, C. Yi, A. K. Chandiran, Md. K. Nazeeruddin, E. W. G. Diau, C. Y. Yeh, S. M. Zakeeruddin and M. Grätzel *Science,* 2011, **334**, 629.

12 a) J. P. Gonzalez-Vazquez, V. Morales-Florez and J. A. Anta *J. Phys. Chem. Lett.,* 2012, **3**, 386; b) T. Dittrich, A. Ofir, S. Tirosh, L. Grinis and A. Zaban *Appl. Phys. Lett.,* 2006, **88**,182110.

13 a) Tan B. and Wu Y. *J. Phys. Chem. B,* 2006, **110**, 15932; b) X. Yan, L. Feng, J. Jia, X. Zhou and Y. Lin *J. Mater. Chem. A,* 2013, **1**, 5347.

14 a) D. K. Roh, W. S. Chi, H. Jeon, S. J. Kim and J. H. Kim *Adv. Func. Mater.,* 2014, **24**, 379; b) N. Memarian, I. Concina, A. Braga, S. M. Rozati, A. Vomiero and G. Sberveglieri *Angew. Chem. Int. Ed.,* 2011, **50**, 12321.

15 a) A.L. Briseno, S.C.B. Mannsfeld, S.A. Jenekhe, Z. Bao and Y. Xia *Materials Today,* 2008, **11**, 38; b) S. Y. Min, T. S. Kim, Y. Lee, H. Cho, W. Xu and T. W. Lee *Small,* 2015, **1**, 45.

16 A. N. Filippin, M. Macias-Montero, Z. Saghi, J. Idigoras, P. Burdet, A. Barranco, P. Midgley, J. A. Anta and A. Borras *Sci. Reports,* 2016, **6**, 20637.

17 a) Y. Oulad-Zian, J. R. Sanchez-Valencia, J. Parra-Barranco, S. Hamad, J. P. Espinos, A. Barranco, J. Ferrer, M. Coll and A. Borras *Langmuir,* 2015, **31**, 8294; b) M. Alcaire, J. R. Sanchez-Valencia, F. J. Aparicio, Z. Saghi, J. C. Gonzalez-Gonzalez, A. Barranco, Y. Oulad-Zian, A. R. Gonzalez-Elipe, P. Midgley, J. P. Espinos, P. Groening and A. Borras *Nanoscale,* 2011, **3**, 4554; c) A. Borras, O. Groening, M. Aguirre, F. Gramm and P. Groening *Langmuir,* 2010, **26**, 5763; d) A. Borras, M. Aguirre, O. Groening, C. Lopez-Cartes and P. Groening *Chem. Mater.,* 2008, **20**, 7371.

18 A. Borras, O. Groening, J. Koeble and P. Groening *Adv. Mater.,* 2009, **21**, 4816.

19 A. Borras, J. R. Sanchez-Valencia, R. Widmer, V. J. Rico, A. Justo and A. R. Gonzalez-Elipe *Crystal Growth Design,* 2009, *9*, 2868.

20 M. Macias-Montero, A. N. Filippin, Z. Saghi, F. J. Aparicio, A. Barranco, J. P. Espinos, F. Frutos, A. R. Gonzalez-Elipe and A. Borras, *Adv. Func. Mater.* 2013, **23**, 5981.

21 K. Moore, C. B. Clemons, K. L. Kreider and G. W. Young *J. Appl. Phys.,* 2007, **101**, 064305.

22 a) L. Ye, J. Mao, L. Liu, Z. Jiang, T. Peng and L. Zan *J. Mater. Chem. A,* 2012, **1**, 10532; b) L. Chu, Z. Qin, J. Yang and Z. Li *Sci. Rep.* 2015, **5**, 12143.

23 a) S. C. Choi, H. S. Lee and S. H. Sohn *Adv. Pow. Technol.,* 2012, *23*, 866; b) F. E. Galvez, P. R. Barnes, J. Halme and H. Miguez *Energy Environ. Sci.,* 2014, **7**, 689.

24 A. G. Vega-Poot, M. Macias-Montero, J. Idigoras, A. Borras, A. Barranco, A. R. Gonzalez-Elipe, F. I. Lizama-Tzec, G. Oskma and J. A. Anta *ChemPhysChem,* 2014, **15**, 1088.

25 V. Gonzalez-Pedro, X. Xu, I. Mora-Sero and J. Bisquert *ACS Nano* 2010, **4**, 5783.

26 J. Idigoras, J. Echeberria, A. Zukal, L. Kavan, O. Miguel, H. J. Grande, J. A. Anta and R. Tena-Zaera *J. Mater. Chem. A,* 2013, **1**, 10173.

27 a) Q. Wang, S. Ito, M. Gratzel, F. Fabregat-Santiago, I. Mora-Sero, J. Bisquert, T. Bessho and H. Imai *J. Phys. Chem. B,* 2006, **110**, 25210; b) J. A. Anta, I. Mora-Sero, T. Dittrich and J. Bisquert *J. Phys. Chem. C,* 2007, **111**, 13997; c) J. A. Anta, I. Mora-Sero, T. Dittrich and J. Bisquert *Phys. Chem. Chem. Phys.,* 2008, **10**, 4478.